Measurements of the edge current evolution during MAST H-modes using MSE

M.F.M. De Bock[1], J. Citrin[2], S. Saarelma[3], D. Temple[3], N.J. Conway[3], A. Kirk[3], H. Meyer[3], C.A. Michael[3] and the MAST team

[1] Eindhoven University of Technology, P.O. Box 513, 5600 MB Eindhoven, The Netherlands
[2] FOM-Institute for Plasma Physics Rijnhuizen, EURATOM/FOM Association, P.O. Box 1207, 3430 BE, Nieuwegein, The Netherlands
[3] EURATOM/CCFE Fusion Association, Culham Science Centre, Abingdon, OX14 3DB, U.K.

Abstract. Edge Localized Modes (ELMs), that are present in most tokamak H-(high confinement) modes, can cause significant damage to plasma facing components in fusion reactors. Controlling ELMs is considered necessary and hence it is vital to understand the underlying physics. The stability of ELMs is typically expressed in terms of the pressure gradient ∇p in the edge and the edge current density j_ϕ. Both ∇p and j_ϕ are usually derived from profiles fitted to the measured edge density and temperature profiles, where for the calculation of j_ϕ neoclassical theory is used.

This paper presents direct measurements of the magnetic pitch angle γ_m evolution in the edge and the derived j_ϕ. On the one hand these provide a method to validate the j_ϕ as derived with neoclassical theory. On the other hand they open up the possibility to find a complete, self-consistent set of edge profiles, that fit both density, temperature and γ_m measurements, hence allowing for a more accurate stability analysis.

1. Introduction

The intermittent energy loss caused by ELM instabilities will cause unacceptable damage to divertor materials in burning plasma fusion reactors like ITER and beyond. Several techniques are investigated to suppress or control ELMs, and for this a good understanding of the ELM stability is needed [1, 2]. Together with the edge pressure gradient ∇p, the stability with respect to ELMs is determined by the edge current density j_ϕ.

Typically j_ϕ is calculated using neoclassical theory, with the bootstrap current being the dominant contribution in the plasma edge [3, 4]. This calculation relies on the profiles of ion and electron temperatures (T_i, T_e) and densities (n_i, n_e) in edge pedestal region. A basic assumption for neoclassical theory is that ion gyroradius ρ_i is significantly smaller than the gradient length L of the profiles $(\rho_i \ll L)$. This condition is, however, not necessarily satisfied in the edge region of an H-mode plasma.

Moreover, because gradients of the input profiles are used in the bootstrap calculation, smooth pedestal profiles are needed. Therefore, edge measurements from e.g. Thomson scattering (TS) or charge exchange recombination spectroscopy (CXRS) are typically fitted by a modified hyperbolic tangent function (mtanh) [5]. However, the mtanh function does not always lead to an acceptable fit to the data. For example in ASDEX Upgrade pedestal proles are better fitted with a piecewise linear function [6]. This means the result of the bootstrap calculation will depend on the choice of fit function.

Finally, the edge measurements need to have a high enough accuracy and radial resolution. Especially for the ion temperature – measured by CXRS, which means the resolution is partly determined by the width of the neutral beam – this can be an issue. In such a case typically $T_i = T_e$ is assumed. Caution is, however, needed with this assumption, because at low collisionality $T_i = T_e$ is typically not valid in the pedestal region [7]. Another assumption often made due to lack of an accurate measurement is $Z_{\text{eff}} = 1$. All assumptions made obviously also have an influence on the final result of the neoclassical determination of j_ϕ in the edge.

The reasons mentioned above call for an independent measurement of the edge j_ϕ that allows to check the validity of the neoclassical calculation. Moreover, such a measurement would also allow to find a complete, self-consistent set of edge profiles, that fit both density, temperature and j_ϕ measurements. When used as input to a stability analysis, this self-consistent set of edge profiles would in turn lead to a more accurate determination of the pedestal stability.

2. Measuring j_ϕ in the plasma edge

Motional Stark effect (MSE) diagnostics are routinely used in tokamaks to derive j_ϕ from the measured the magnetic pitch angle $\gamma_m = \arctan(B_\theta/B_\phi)$, with B_θ the poloidal and B_ϕ the toroidal magnetic field [8]. Because γ_m depends on the integrated current,

measuring a change of j_ϕ in the edge is difficult, as j_ϕ has to compete with the total plasma current in order to cause a noticeable change in γ_m. Moreover, MSE depends on the local radial electric field E_r as well, which can be large in the pedestal region during H-mode. Techniques other than MSE have been used for edge current measurements, but typically long integration times are necessary (~ 100 ms) [9]. A very recent method based on electron Bernstein wave emission looks promising in terms of spatial and time resolution, but requires complicated data analysis [10].

γ_m relates to j_ϕ through B_θ and Ampère's law. A change $\Delta\gamma$ due to a change in j_ϕ is given by:

$$\Delta\gamma_m = \frac{B_\phi \Delta B_\theta}{B_\theta^2 + B_\phi^2}. \tag{1}$$

This means that in devices with a similar poloidal field B_θ but a lower toroidal field B_ϕ compared with conventional tokamaks, $\Delta\gamma_m$ will be larger and hence changes in the edge j_ϕ easier to detect. For the spherical tokamak MAST $B_\phi \approx 0.25$ T at the low field side edge, whereas $B_\theta \approx 0.2$ T. In a MAST H-mode a 10% bootstrap fraction is not unreasonable, which means an increase of $\Delta B_\theta \approx 0.02$ T over the pedestal. The resulting change in pitch angle according to (1) would thus be $\Delta\gamma_m \approx 3°$. At 2 ms time resolution the MAST MSE system is capable of resolving this expected change in γ_m [11, 12, 13].

An MSE diagnostic does not measure γ_m directly, but instead measures a polarization angle γ that in absence of a radial electric field E_r is proportional to γ_m. When E_r cannot be neglected, as is the case in the H-mode pedestal, a correction for E_r is necessary. For an up-down symmetric plasma with the MSE measurements taken in the mid plane ($Z = 0$), which is the case for the MAST discharge presented in this paper (#24409), $B_\theta = B_Z$ and the angle γ measured by the MSE diagnostic is:

$$\tan(\gamma) = \frac{-\cos(\beta)B_z - (E_r/v)\cos(\alpha + \beta)}{\sin(\alpha)B_\phi}, \tag{2}$$

with the angles α and β describing the neutral beam and viewing geometry and v the beam velocity. By using equation (2) to constrain the equilibrium reconstruction in codes like EFIT B_Z and j_ϕ can be found [14]. However, the basis functions used in the EFIT code have difficulties dealing with the strong pressure gradient of the H-mode pedestal, resulting in an inaccurate fitting to the MSE data, as can be seen in figure 1. A more accurate result, including an estimate of the error, can be obtained by calculating B_Z directly from the MSE angle γ and then use Ampère's law to derive j_ϕ [15]:

$$\mu_0 j_\phi = \frac{\partial B_R}{\partial Z} - \frac{\partial B_Z}{\partial R}. \tag{3}$$

B_ϕ, E_r and $\partial B_R/\partial Z$ are unknowns in equations (2) and (3) and will be discussed below. Figure 1 shows profiles of γ and the corresponding j_ϕ in L- and H-mode, both from a MSE constrained EFIT reconstruction (dotted lines) and as derived from the MSE data directly (full lines with shaded error bars). Clearly an increase of γ near the last closed
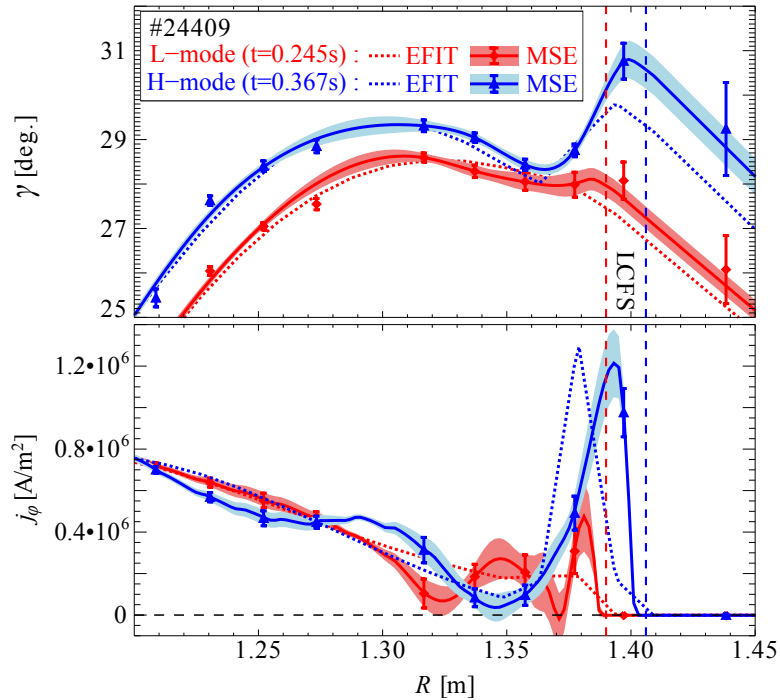
Figure 1. (Color online) Profiles of γ and j_ϕ during L-mode and H-mode. The dotted lines are the result of an EFIT equilibrium reconstruction, the full lines with (shaded) error bars are MSE measurements of γ (top) and j_ϕ derived from γ directly using Ampère's law (bottom). In H-mode a clear peaking of γ and j_ϕ are observed in the edge.

flux surface (LCFS) is observed for the H-mode phase, and consequently a peak in the edge current.

The value of B_ϕ needed in equation (2) is taken from an initial EFIT reconstruction. This can be done because B_ϕ is only weakly dependent on the local j_ϕ in the edge. An extra check on B_ϕ is that it has to be close to the well known vacuum toroidal field in the edge of the plasma.

E_r is derived from the ion fluid as:

$$E_r = -v_\phi \times B_Z + v_Z \times B_\phi + \frac{\nabla(n_i\, T_i)}{e\, n_i}, \tag{4}$$

where v_ϕ and v_Z are the toroidal and poloidal plasma rotation in the mid plane and T_i and n_i are the ion temperature and density. In this discharge T_i and v_ϕ are measured with CXRS and n_i is assumed to be equal to the electron density n_e measured with Thomson scattering [16, 17]. No measurement of v_Z exists for this discharge, but it was observed in other discharges that v_Z is, even in H-mode, an order of magnitude lower then v_ϕ [18]. With B_ϕ being of the order of B_Z at the low field side edge of the MAST tokamak, the term $v_Z \times B_\phi$ can be neglected with respect to the $v_\phi \times B_Z$ term.

In the plasma edge the spatial resolution of the CXRS diagnostic is insufficient to
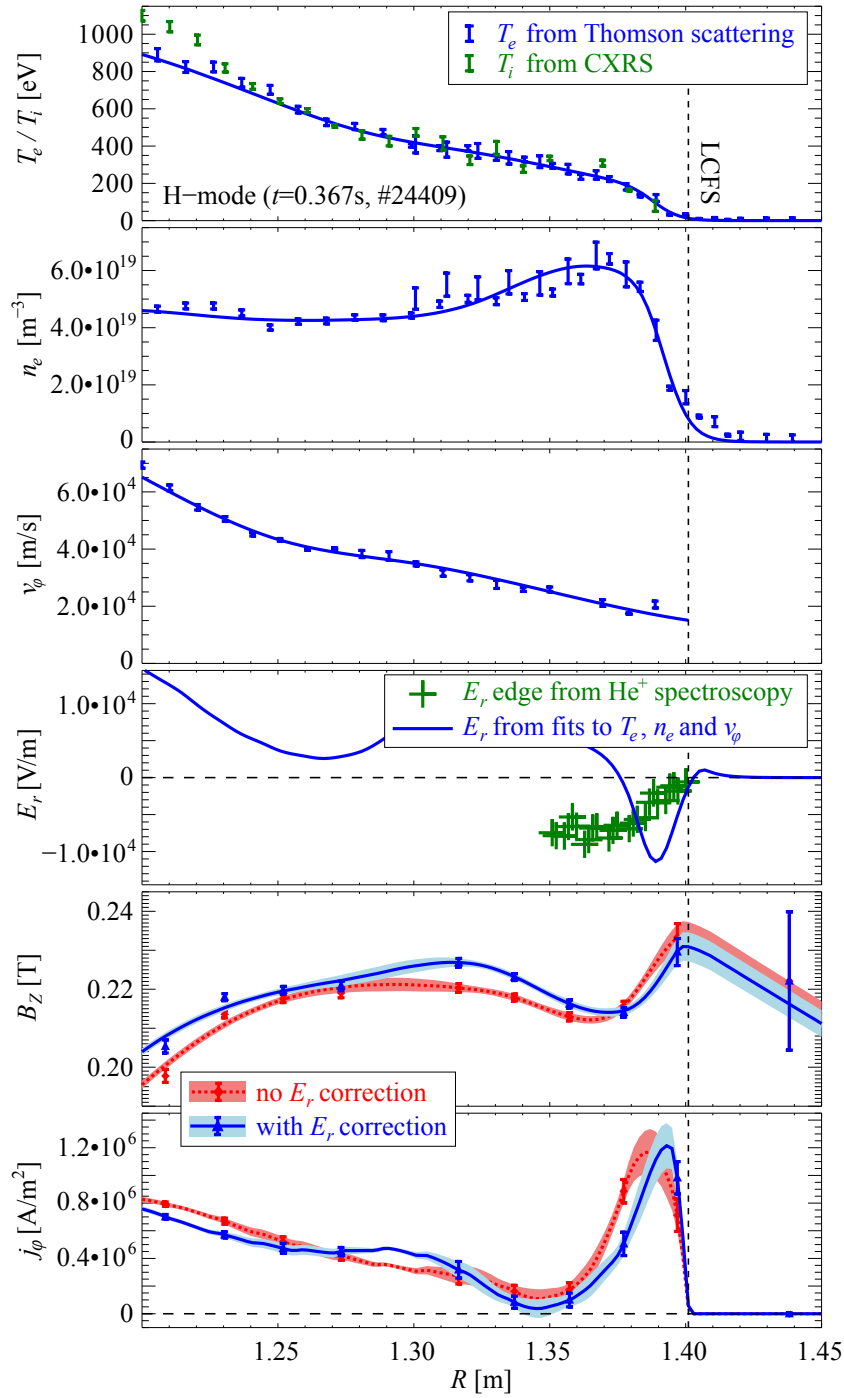
Figure 2. (Color online) The top plot shows the used E_r (full line) and the He$^+$ spectroscopic measurement for the edge (crosses). Middle and bottom plots show B_Z and j_ϕ with and without E_r correction. The effect of E_r is only small.

calculate $\nabla(n_e T_i)$. Here the assumption $T_i = T_e$ was made. In the first plot of figure 2 measurements of both T_e from Thomson scattering and T_i from CXRS are shown. For the discharge under investigation the assumption $T_i = T_e$ in the plasma edge is justified. With the above assumption (4) becomes:

$$E_r = -v_\phi \times B_Z + \frac{\nabla(n_e T_e)}{e\, n_e}, \tag{5}$$

To calculate E_r the measurement data was fitted with a mtanh function over the pedestal (normalized poloidal flux $\psi > 0.7$) continously connected to a spline fit of the core data. Except for v_ϕ, that shows no evidence of a pedestal-like profile and was fitted with a spline only. The fits to the measurement data of T_e, n_e and v_ϕ are shown as full lines in the top three plots of figure 2.

Solving (5) and (2) returns E_r and B_Z. The full line in the fourth plot of figure 2 shows the hence calculated E_r. In the same plot an independent measurement of E_r in the plasma edge is shown (crosses). These measurements were obtained from Doppler spectroscopy measurements on He$^+$ injected into the plasma edge [19]. The resulting E_r is of the same amplitude but is located over a wider region than the E_r based on TS and CXRS measurements. A wide, flat E_r profile, however, results in a shift of the B_Z profile (see (2)), but does not change the gradient of B_Z and hence has little influence on j_ϕ (see (3)). This means that by using the E_r based on TS and CXRS measurements, if anything, the effect of E_r is overestimated. Nonetheless, even this overestimated effect on B_Z and j_ϕ is very small. This can be seen in the bottom two plots of figure 2 where the B_Z and j_ϕ profiles both with and without E_r correction are shown. Uncertainties in the determination of E_r are therefore not considered a major point of concern at MAST.

Finally the term $\partial B_R/\partial Z$ in Ampere's can be found from the initial EFIT reconstruction. Taking into account the flux surface shape depends only weakly on the local j_ϕ, it can be assumed that: $B_Z/B_R \approx B_Z^{\text{EFIT}}/B_R^{\text{EFIT}}$. From this easily follows:

$$\frac{\partial B_R}{\partial Z} = \frac{B_Z}{B_Z^{\text{EFIT}}} \frac{\partial B_R^{\text{EFIT}}}{\partial Z}. \tag{6}$$

B_Z can be calculated for every MSE channel and its error can be derived from the measurement error in γ. The data points with error bars in the fifth plot of figure 2 indicate this. However, for the gradient of B_Z needed in (3) the spatial resolution of the MSE diagnostic is too coarse. Therefore, smooth γ-profiles were obtained by fitting a spline to the measured γ. These smooth γ-profiles were then used to calculate smooth B_Z and j_ϕ profiles using equations (2), (3) and (5), indicated by the full lines in the bottom two plots of figure 2.

As an estimate for the errors, a set of splines was fitted to the measured γ perturbed by its errors. For each perturbed spline B_Z and j_ϕ was calculated and the r.m.s. determines the error. This is indicated by the shaded areas around the profiles shown in figures 1, 2 (bottom two plots), 3 and 4.
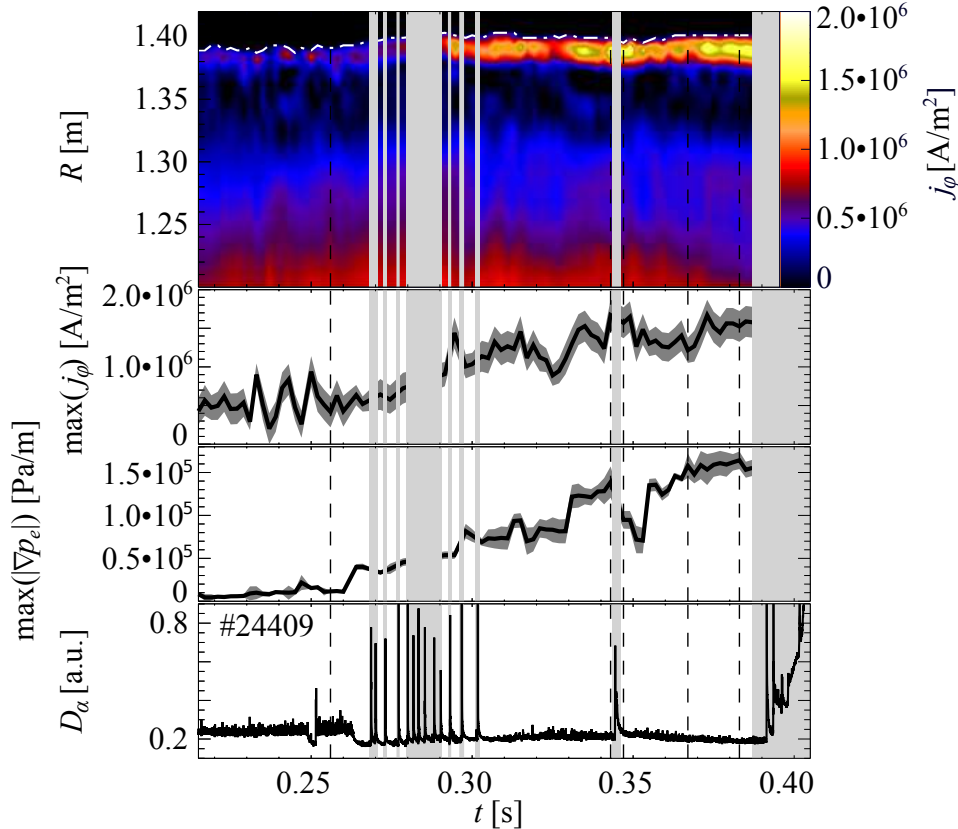
Figure 3. (Color online) The evolution of j_ϕ, $\max(|\nabla p_e|)$ and the D_α emission. The position of the LCFS is indicated in the contour plot by the white —· line. The vertical dashed lines indicate the profiles shown in figures 1, 2 and 4.

3. The evolution of j_ϕ in the plasma edge

Figure 3 shows the evolution of j_ϕ, $\max(|\nabla p_e|)$ and the D_α emission during the discharge. The periods around the ELMs are blocked by grey areas because no reliable MSE measurement exists at those times.

The L-H transition into a high frequency, type III ELMy H-mode occurs at $t = 0.263$ s. Apart from one outlier at $t = 0.295$ s the edge j_ϕ gradually increases during this type III phase and so does $\max(|\nabla p_e|)$. This is consistent with the picture of pressure driven edge current. However, due to the short inter-ELM period typically only one j_ϕ profile can be obtained per ELM period. Hence, no information can be obtained about the inter-ELM evolution of j_ϕ.

The focus of the discussion will therefore lie on the 2 long ELM-free periods following the type III phase: starting at $t = 0.302$ s and separated by a type I ELM at $t = 0.345$ s. A final ELM at $t = 0.392$ s terminates the H-mode, quickly followed by a disruption.

During these ELM-free periods strong currents are observed in the plasma edge. The edge current is located at the pedestal position, about 2-3 cm just inside the last

closed flux surface. The amplitude of the edge j_ϕ reaches up to 1.6 MA/m^2, which is in the order of the central current density.

On average $\max(j_\phi)$ increases with increasing $\max(|\nabla p_e|)$. However, the changes in $\max(j_\phi)$ are less abrupt than those in $\max(|\nabla p_e|)$ and are delayed several milliseconds with respect to the changes in $\max(|\nabla p_e|)$. Two examples of this are:

- The sudden increase of $\max(|\nabla p_e|)$ at $t = 0.329$ s is accompanied by a much more gradual increase of $\max(j_\phi)$.

- At the ELM crash ($t = 0.345$ s) $\max(|\nabla p_e|)$ drops significantly whereas $\max(j_\phi)$ remains high for ~ 4 ms (up to $t = 0.349$ s), after which it only decreases gradually.

Other interesting observations are the decrease of $\max(j_\phi)$ in periods where $\max(|\nabla p_e|)$ remains more or less constant. This happens from $t = 0.317$ s to $t = 0.327$ s, and again from $t = 0.335$ s to $t = 0.341$ s (just before the ELM).

The delays and more gradual evolution of j_ϕ suggest that current diffusion plays an important role. Another influence could be the collisionality [20]. This because the pedestal pressure in MAST is strongly dominated by the density (see figure 2). In the next section both will be investigated.

4. Comparison with neoclassical bootstrap calculation and current diffusion

The edge j_ϕ during H-mode is typically attributed to the high bootstrap current fraction due to the large pressure gradient. In the previous section it was shown that indeed the measured j_ϕ on average increases with increasing ∇p_e. For a more detailed comparison, however, a full neoclassical calculation needs to be done.

In such a full calculation the current comes from the bootstrap drive, including the effect of collisionality, but also the inductively driven part, because the pedestal profiles also change the resistivity. Finally the calculated current has to be part of a self-consistent equilibrium.

Two codes were used to calculate the edge j_ϕ based on the profiles of T_e, T_i and n_e. Again $T_i = T_e$ was assumed for the pedestal and $Z_{\mathrm{eff}} = 1$ was assumed over the whole plasma.

First code used is the HELENA equilibrium code, where the the formulas of [3, 4] are included for the bootstrap calculation [21]. HELENA treats every time frame separately and therefore does not include current diffusion.

The second code is the CRONOS suite [22]. This suite of codes also uses HELENA for the equilibrium, but calculates the bootstrap current drive with NCLASS [23]. Furthermore, the CRONOS suite does include the current diffusion calculation.

Figure 4 shows a comparison between j_ϕ derived from MSE and j_ϕ calculated by HELENA and CRONOS for 3 time points: just before the ELM ($t = 0.347$ s), just after the ELM ($t = 0.347$ s) and late in the ELM-free period ($t = 0.383$ s). Because the calculations of both HELENA and CRONOS return the complete equilibrium, and hence profiles of B_Z and B_ϕ, equations (2) and (5) can be used to calculate the expected MSE
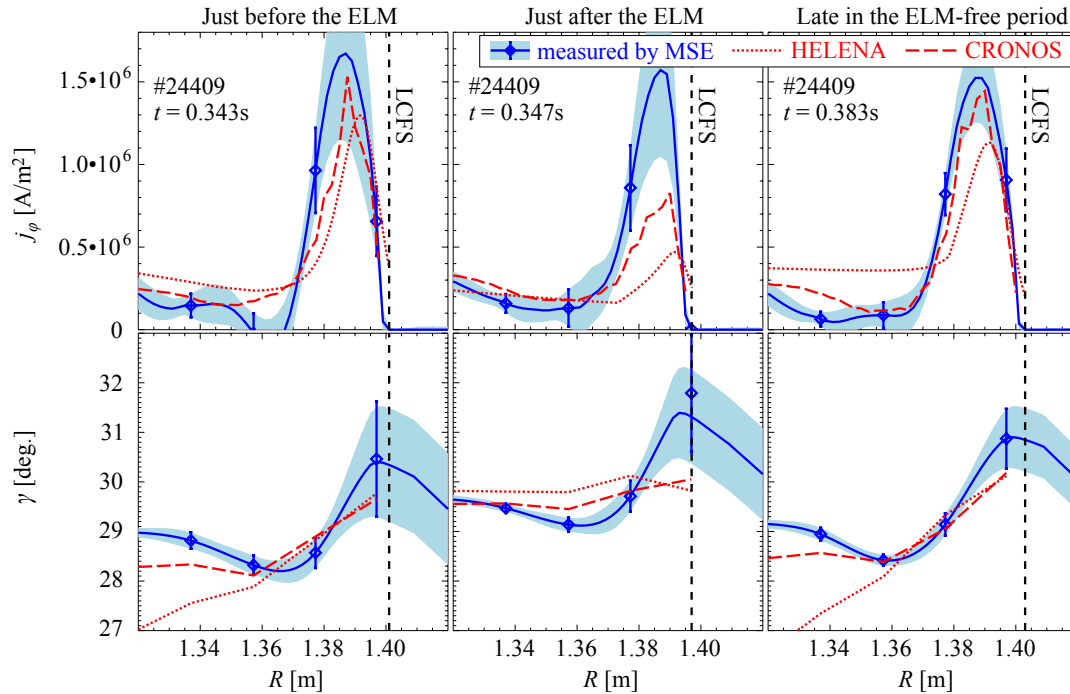
Figure 4. Comparison of the neoclassical calculation and the MSE measurement of γ (bottom) and j_ϕ (top). Just after the ELM the calculation predicts significantly less edge current than that measured. Late in the ELM-free period the agreement is better.

angles γ_{HELENA} and γ_{CRONOS}. These can then be directly compared with the γ-profiles measured by MSE. This more straightforward comparison is also shown in figure 4.

One observes that just before the ELM and long after the ELM both the HELENA and the CRONOS calculations are in good agreement with the measurements. Where CRONOS, being the more elaborate model, also gives better agreement in the core of the plasma (not shown in the figure).

Just after the ELM, however, the agreement is worse, especially for the HELENA code. The inclusion of current diffusion in CRONOS does lead to a slightly higher current, but enough to agree with the MSE measurement. It seems as if current diffusion is indeed the key factor, but that the actual current diffusion is slower than what the neoclassical theory predicts. In other words, the neoclassical resistivity seems too large. This has been observed in previous experiments on current diffusion as well, wheret was suggested that Spitzer resistivity agrees better with the experimental evidence [24, 25].

Just before the ELM and late in the second ELM-free period both HELENA and CRONOS give the same result for γ in the edge, indicating that by then the edge current is fully relaxed. Despite agreeing within the error bars with the measured γ, the gradients of γ_{HELENA} and γ_{CRONOS}, and hence the calculated currents, are even at these times slightly lower than measured ones. This the case throughout the discharge. Possible reasons for this difference could be:

(a) The fact that neoclassical theory is not fully valid, because $\rho_i \ll L$ in the H-mode
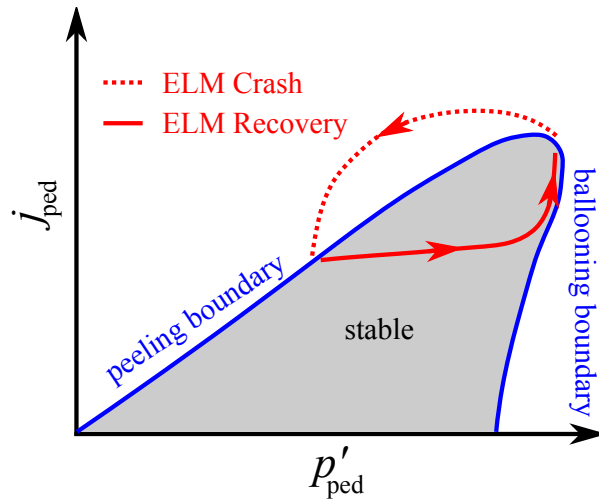
Figure 5. (Color online) Simplified model of the type I ELM cycle according to the peeling-ballooning model. The pressure gradient builds up until the ballooning boundary is reached. The pedestal current can then still rise due to current diffusion until also the peeling boundary is reached. At that point the peeling-ballooning mode are destabilized and the ELM crash occurs (figure adapted from [27]).

edge.

(b) Certain elements that are not included in the neoclassical model, such as the enhancement of the bootstrap current due to E_r [26].

(c) The fact that the functions fitted to the T_i, T_e and n_e measurements do not describe the pedestal profiles accurately enough.

The latter means that by e.g. integrated data analysis it would be possible to find pedestal profiles that fit the measured T_i, T_e, n_e and γ. Such profiles would then give a better and self-consistent description of the pedestal. When using these profiles as an input to stability analysis, more reliable results would be obtained.

5. Notes on stability

The stability of the H-mode pedestal with respect to ELM can be described by the peeling-ballooning model [27]. It descibes a stability region in terms of the pedestal pressure gradient p'_{ped} and current j_{ped}. A simplified picture of the model is shown in figure 5 (figure adapted from [27]). If the pressure gradient exceeds a certain threshold ballooning modes are destabilized (the ballooning boundary). The pedestal currents j_{ped}, however, reduce the edge magnetic shear, which in turn stabilizes the ballooning modes and shifts the ballooning boundary to higher values of p'_{ped}. On the other hand increasing j_{ped} will provide free energy that can destabilize peeling modes (the peeling boundary). When crossing the threshold at both high p'_{ped} and high j_{ped}, where the peeling and ballooning boundaries meet, coupled peeling-ballooning modes are destabilized.
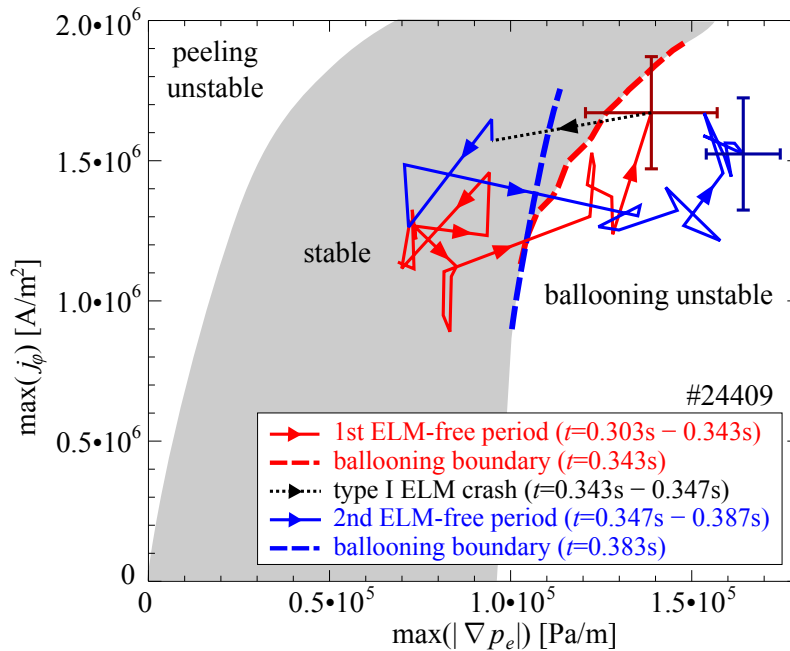
Figure 6. (Color online) $\max(j_\phi)$ is plotted versus $\max(|\nabla p_e|)$ showing the stability evolution . The ballooning boundary (thick, dashed lines) was calculated using ELITE at $t = 0.343$ s and $t = 0.383$ s. For these time frames also the errors of $\max(j_\phi)$ and $\max(|\nabla p_e|)$ are indicated (error bars are of similar size for the other data points). The peeling boundary of the stable region (top left) is indicative only as no unstable peeling modes were found in the vicinity of the data points at $t = 0.343$ s or $t = 0.383$ s.

Figure 5 also illustrates schematically a type I ELM cycle: p'_{ped} increases during the inter-ELM period and saturizes near the ballooning boundary. j_{ped} also rises, but more slowly due to current diffusion. This means j_{ped} still grows when p'_{ped} has already fully recovered. At high enough j_{ped} the stability boundary is then crossed and peeling-ballooning modes destabilized, leading to the ELM crash.

However, detailed study at ASDEX upgrade of the inter-ELM evolution of n_e and T_e profiles showed that the slow build-up of the derived edge j_ϕ found from neoclassical current diffusion calculations cannot explain the gap between the saturation of $\max(|\nabla p_e|)$ and the onset of the ELM [28]. Again a possible explanation could be that the actual current diffusion is possible slower than neoclassically calculated (see previous section). However, also in the MAST discharge presented in this paper both the measured $\max(|\nabla p_e|)$ and the measured $\max(j_\phi)$ are saturated well before the ELM, especially near the end of the second ELM-free period ($t > 0.375$ s). This can be seen in figure 3.

In figure 6 the measured $\max(j_\phi)$ is plotted against the measured $\max(|\nabla p_e|)$. I.e. the experimental version of the simplified stability plot of figure 5. Ideally a stability analysis should be performed for every data point in the figure. This, however, falls out of the scope of this paper. Therefore a stability analysis was done only for the time frames at $t = 0.343$ s (just before the ELM) and $t = 0.383$ s (near the end of the

discharge). The stability calculations were done for toroidal mode numbers 5-30 using the ELITE code [29, 27].

At $t = 0.343$ s the plasma is found to be marginally unstable against ballooning modes. The calculated stability boundary, indicated by the red dashed line in figure 6, lies within the error bars of the data point. During the first ELM free period, i.e. up to $t = 0.343$ s, the $(\max(|\nabla p_e|), \max(j_\phi))$ data points evolve more or less along the ballooning boundary towards higher $\max(j_\phi)$; in agreement with the peeling-ballooning model. The only caveat is that at the ELM-crash only ballooning modes, rather than peeling-ballooning modes, are found to be unstable.

At $t = 0.383$ s both $\max(|\nabla p_e|)$ and $\max(j_\phi)$ are saturated. Moreover, the ELM does not occur until 10 ms later, at $t = 0.392$ s (when no MSE measurements were available anymore). This indicates that the plasma is (at least marginally) stable. The ELITE stability analysis, however, predicts that the plasma should be strongly unstable against ballooning modes, with the calculated stability boundary, indicated by the blue dashed line in figure 6, well outside the error bars of the data point. This clearly does not agree with the observed stable plasma at $t = 0.383$ s.

Because the calculated stability depends strongly on both the shape of the plasma cross section, as well as on the pressure and current proles, it is possible that the used profiles do not accurately enough describe the pedestal. This could lead to a false prediction on the stability. Again this calls for an accurate, self-consistent description of the pedestal profiles that fits the measurements of both T_i, T_e, n_e and γ.

6. Summary and conclusion

Both bootstrap current and stability calculations depend strongly on the quality of and assumptions on the input profiles. Independent measurements of the current in the plasma edge would allow for a better description of the plasma pedestal, a validation of neoclassical bootstrap current and finally a more accurate determination of the stability with respect to ELMs.

Thanks to a large pitch angle and a small E_r correction, MSE can be used as tool for routinely measuring the edge j_ϕ evolution in spherical tokamaks. First measurements show neoclassical calculations approximately agree with measurements when the edge current is fully relaxed. Just after the ELM event, however, the current remains high for several milliseconds. This is longer than what is found from current diffusion calculations using neoclassical resistivity. The evolution j_ϕ and ∇p_e in a stability plot shows that both j_ϕ and ∇p_e can be fully relaxed well before the ELM crash. This does not agree with the hypothesis that ∇p_e can only be saturated before the ELM onset as long as j_ϕ still rises (e.g. due to current diffusion). Preliminary stability calculations also falsely predict unstable conditions well before ELM onset.

Further work could be done, e.g. by integrated data analysis, on determining pedestal profiles that fit both the measured T_i, T_e, n_e profiles and the measured γ-profiles for MSE. Such profiles would then give a better and self-consistent description

of the pedestal. Furthermore, when using these profiles as an input to stability analysis, more reliable results could be obtained.

Acknowledgments

[1] T. E. Evans, R. A. Moyer, P. R. Thomas, J. G. Watkins, T. H. Osborne, J. A. Boedo, E. J. Doyle, M. E. Fenstermacher, K. H. Finken, R. J. Groebner, M. Groth, J. H. Harris, R. J. La Haye, C. J. Lasnier, S. Masuzaki, N. Ohyabu, D. G. Pretty, T. L. Rhodes, H. Reimerdes, D. L. Rudakov, M. J. Schaffer, G. Wang, and L. Zeng. Suppression of large edge-localized modes in high-confinement diii-d plasmas with a stochastic magnetic boundary. *Physical Review Letters*, 92(23):235003–1–235003–4, 2004.
[2] P. T. Lang, J. Neuhauser, L. D. Horton, T. Eich, L. Fattorini, J.C. Fuchs, O. Gehre, A. Herrmann, P. Ignácz, M. Jakobi, S. Kálvin, M. Kaufmann, G. Kocsis, B. Kurzan, C. Maggi, M.E. Manso, M. Maraschek, V. Mertens, A. Mück, H.D. Murmann, R. Neu, I. Nunes, D. Reich, M. Reich, S. Saarelma, W. Sandmann, J. Stober, U. Vogl, and the ASDEX Upgrade Team. Elm frequency control by continuous small pellet injection in asdex upgrade. *Nuclear Fusion*, 43(10):1110, 2003.
[3] O. Sauter, C. Angioni, and Y. R Lin-Liu. Neoclassical conductivity and bootstrap current formulas for general axisymmetric equilibria and arbitrary collisionality regime. *Physics of Plasmas*, 6(7):2834, 1999.
[4] O. Sauter, C. Angioni, and Y. R Lin-Liu. Erratum: neoclassical conductivity and bootstrap current formulas for general axisymmetric equilibria and arbitrary collisionality regime [phys. plasmas 6, 2834 (1999)]. *Physics of Plasmas*, 9(12):5140, 1999.
[5] R. J. Groebner, M. A. Mahdavi, A. W. Leonard, T. H. Osborne, and G. D. Porter. Role of neutrals in density pedestal formation in diii-d. *Plasma Physics and Controlled Fusion*, 44(5A):A265, 2002.
[6] P. A. Schneider, E. Wolfrum, B. Kurzan, and H. Zohm. Alternative method for characterization of inter-elm edge profiles of type i elmy h-modes in asdex up. In *37th EPS Conference on Controlled Fusion and Plasma Physics*, pages P–2.157. EPS, 2010.
[7] T. Morgan, H. Meyer, D. Temple, and G. Tallents. A new edge ion temperature measurement diagnostic on the mast tokamak. In *37th EPS Conference on Controlled Fusion and Plasma Physics*, pages P–5.122. EPS, 2010.
[8] F. M. Levinton, R. J. Fonck, G. M. Gammel, R. Kaita, H. W. Kugel, E. T. Powell, and D. W. Roberts. Magnetic field pitch-angle measurments in the pbx-m tokamak using the motional stark effect. *Physical Review Letters*, 63:2060–2063, 1989.
[9] D. M. Thomas, A. W. Leonard, L. L. Lao, T. H. Osborne, H. W. Mueller, and D. K. Finkenthal. Measurement of pressure-gradient-driven currents in tokamak edge plasmas. *Physical Review Letters*, 93:065003, 2004.
[10] V. F. Shevchenko, M. F. M. De Bock, S. J. Freethy, A. N. Saveliev, and R. G. L. Vann. Two-dimensional studies of electron bernstein wave emission in mast. *Fusion Science and Technology*, 59(4):663, 2011.
[11] M. F. M. de Bock, N. J. Conway, M. J. Walsh, P. G. Carolan, N. C. Hawkes, and the MAST Team. Ab initio modeling of the motional stark effect on mast. *Review of Scientific Instruments*, 79(10):10F524, 2008.

[12] M. F. M. De Bock, C. A. Michael, N. J. Conway, L. Appel, I.T. Chapman, M. Gryaznevich, H. Tojo, and M. R. Turnyanskiy. First multi-chord mse measurements on mast. In ECA, editor, *36th EPS Conference on Controlled Fusion and Plasma Physics*, volume 33E, pages P–5.186. EPS, 2009.

[13] N. J. Conway, M. F. M. De Bock, C. A. Michael, M. J. Walsh, P. G. Carolan, N. C. Hawkes, E. Rachlew, J. F. G. McCone, Shibaev S., and G. Wearing. The mast motional stark effect diagnostic. *Review of Scientific Instruments*, 81(10):10D738, 2010.

[14] L. C. Appel, G. T. A. Huysmans, L. L. Lao, P. J. McCarthy, D. G. Muir, E. R. Solano, J. Storrs, D. Taylor, W. Zwingmann, and contributors to the EFDA Integrated Tokamak Modelling (ITM) Task Force and JET-EFDA Contributors. A unified approach to equilibrium reconstruction. In ECA, editor, *33rd EPS Conference on Controlled Fusion and Plasma Physics*, volume 30C, pages P–2.184. EPS, 2006.

[15] C. C. Petty, Y. R Lin-Liu, T. C. Luce, M. A. Makowski, R. Prater, D. I. Schuster, H. E. St. John, and K. L. Wong. Localized measurements of electron cyclotron current drive using mse spectroscopy on the diii-d tokamak. *Nuclear Fusion*, 41(5):551, 2001.

[16] N. J. Conway, P. G. Carolan, J. McCone, M. J. Walsh, and M. Wisse. High-throughput charge exchange recombination spectroscopy system on mast. *Review of Scientific Instruments*, 77:10F131, 2006.

[17] R. Scannell, M. J. Walsh, M. R. Dunstan, J. Figueiredo, G. Naylor, T. O'Gorman, S. Shibaev, K. J. Gibson, and H. Wilson. A 130 point nd:yag thomson scattering diagnostic on mast. *Review of Scientific Instruments*, 81(10):10D520, 2010.

[18] A. R. Field, J. McCone, N. J. Conway, M. Dunstan, S. Newton, and M Wisse. Comparison of measured poloidal rotation in mast spherical tokamak plasmas with neo-classical predictions. *Plasma Physics an*, 51:105002, 2009.

[19] H. Meyer, C. Bunting, P. G. Carolan, N. J. Conway, M. R. Dunstan, A. Kirk, R. Scannell, D. Temple, M. Walsh, and the MAST and NBI Teams. The structure, evolution and role of the radial edge electric field in h-mode and l-mode on mast. *Journal of Physics: Conference Series*, 123:012005, 2008.

[20] D. M. Thomas, A. W. Leonard, T. H. Osborne, R. J. Groebner, W. P. West, and K. H. Burrell. The effect of plasma collisionality on pedestal current density formation in diii-d. *Plasma Physics and Controlled Fusion*, 48:A183–A191, 2006.

[21] G.T.A. Huysmans, J.P. Goedbloed, and W.O.K. Kerner. In *Computational Physics (Proc. Int. Conf. Amsterdam)*, page 371. World Scientific Publishing, Singapore, 1991.

[22] J. F. Artaud, V. Basiuk, F. Imbeaux, M. Schneider, J. Garcia, G. Giruzzi, P. Huynh, T. Aniel, F. Albajar, J. M. Ané, A. Bécoulet, C. Bourdelle, A. Casati, L. Colas, J. Decker, R. Dumont, L.-G. Eriksson, X. Garbet, R. Guirlet, P. Hertout, G. T. Hoang, W. A. Houlberg, G. Huysmans, E. Joffrin, S. H. Kim, F. Köchl, J. Lister, X. Litaudon, P. Maget, R. Masset, B. Pégourié, Y. Peysson, P. Thomas, E. Tsitrone, and F. Turco. The cronos suite of codes for integrated tokamak modelling. *Nuclear F*, 50(4):043001, April 2010.

[23] W.A. Houlberg, K. C. Shaing, S. P. Hirshman, and M. C. Zarnstorff. Bootstrap current and neoclassical transport in tokamaks of arbitrary collisionality and aspect ratio. *Physics of Plasmas*, 4:3230, 1997.

[24] I. Jenkins, M. Baruzzo, M. Brix, C. D. Challis, N. C. Hawkes, X. Litaudon, J. Mailloux, F. G. Rimini, P.C. de Vries, and JET-EFDA Contributors. Test of current ramp modelling for at regimes in jet. In *37th EPS Conference on Controlled Fusion and Plasma Physics*, pages P–2.178. EPS, 2010.

[25] D. D. Keeling, R. J. Akers, M. F. M. De Bock, C. D. Challis, C. A. Michael, A. Patel, and the MAST team. Test of current diffusion modelling in mast current ramp-up. In *38th EPS Conference on Controlled Fusion and Plasma Physics*, pages P–2.178. EPS, 2011.

[26] Grigory Kagan and Peter J. Catto. Enhancement of the bootstrap current in a tokamak pedestal. *Physical Review Letters*, 105:045002, July 2010.

[27] P.B. Snyder, H.R. Wilson, J.R. Ferron, L.L. Lao, A.W. Leonard, T.H. Osborne, A.D. Turnbull, D. Mossessian, M. Murakami, and X.Q. Xu. Edge localized modes and the pedestal: A model based on coupled peelingballooning modes. *Physics of Plasmas*, 9:2037, 2002.

[28] A. Bruckhart, E. E. Wolfrum, R. Fischer, K. Lackner, H. Zohm, and the ASDEX Upgrade Team. Inter-elm behaviour of the electron densitiy and temperature pedestal in asdex upgrade. *Plasma Physics and Controlled Fusion*, 52:105010, 2010.

[29] H.R. Wilson, P.B. Snyder, G.T.A. Huysmans, and R.L. Miller. Numerical studies of edge localized instabilities in tokamaks. *Physics of Plasmas*, 9:1277, 2002.